RECENT ADVANCES IN TRANSPORT MODELING FOR MINIATURIZED CMOS DEVICES (INVITED)

T. Grasser, A. Gehring, and S. Selberherr
Institute for Microelectronics, TU Vienna
Gusshausstr. 27–29, A-1040 Vienna, Austria
E-mail: Tibor.Grasser@iue.tuwien.ac.at

Abstract — With the rapid feature size reduction of modern semiconductor devices accurate description of hot-carrier phenomena is becoming very important. Frequently used carrier transport models are the traditional drift-diffusion model and energy-transport models which also consider the average carrier energy as an independent solution variable. Recent results show, however, that the average energy is in many cases not sufficient for accurate modeling. Both the transport models themselves and the models for the physical parameters seem to be affected. After a review of the conventional models we present highly accurate impact ionization and gate current models based on a six moments transport model.

I. INTRODUCTION

Numerical simulation of carrier transport in semiconductor devices dates back to the famous work of Scharfetter and Gummel [1]. Since then the transport models have been continously refined and extended to more accurately capture transport phenomena occurring in modern semiconductor devices. The need for refinement and extension is primarily caused by the ongoing feature size reduction in state-of-the-art technology. As the supply voltages cannot be scaled accordingly without jeopardizing the circuit performance, the electric fields inside the devices have increased. Large electric fields which rapidly change over small length scales give rise to non-local and hot-carrier effects which begin to dominate device performance. An accurate description of these phenomena is required and is becoming a primary concern for industrial applications.

Transport equations used in semiconductor device simulation are normally derived from Boltzmann's transport equation which provides a semiclassical description of carrier transport. Boltzmann's equation needs to be solved in the seven-dimensional phase space which is prohibitive for engineering applications. Monte Carlo simulations have been proven to give accurate results but are restrictively time consuming. Furthermore, if the distribution of high-energetic carriers is relevant, or if the carrier concentration is very low in specific regions of the device, Monte Carlo simulations tend to produce high variance in the results. Therefore, a common simplification is to investigate only some moments of the distribution function, such as the carrier concentration and the carrier temperature.

Beside the classic drift-diffusion model, moment based transport models have been proposed which consider the carrier energy an independent solution variable [2], [3], [4], [5]. These models are capable of describing non-local and hot-carrier effects to a first order. Recent results, however, suggest that the average energy is in many cases not sufficient for accurate modeling. Even more important is the fact that models based solely on the average carrier energy can give results worse than those obtained by models that omit this effect. To solve this apparent discrepancy it has been suggested to include the average square energy into the transport models [6], [7]. This results in a six moments transport model and some of its benefits will be discussed in this article.

II. THE DRIFT-DIFFUSION MODEL

The drift-diffusion model is the simplest current transport model which can be derived from Boltzmann's transport equation by the method of moments [8] or from basic principles of irreversible thermodynamics [9]. It has been the working horse in industrial applications for over thirty years. Within the drift-diffusion model the well known continuity and current equations have to be solved which read in their static form

$$\nabla \cdot \mathbf{J} = \mathrm{q}R$$
$$\mathbf{J} = \mathrm{q}\mu n\mathbf{E} + \mu \mathrm{k_B} T_\mathrm{L} \nabla n$$

Here, μ denotes the electron mobility, T_L the lattice temperature, $\mathbf{E}$ the electric field, and R the recombination rate.

In the drift-diffusion approach the local temperature of the carrier gas can be estimated via the homogeneous energy balance equation

$$T_n = T_\mathrm{L} + \tfrac{2}{3}\tfrac{\mathrm{q}}{\mathrm{k_B}}\tau_\mathcal{E}\mu\mathbf{E}^2 \qquad (1)$$

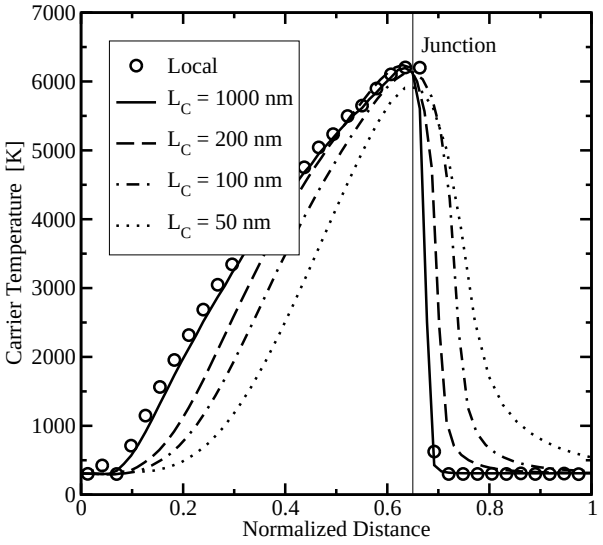

Fig. 1: The carrier temperature of comparable n^+-n-n^+ test structures with varying channel lengths where the spatial coordinates have been normalized to get an overlapping electric field.

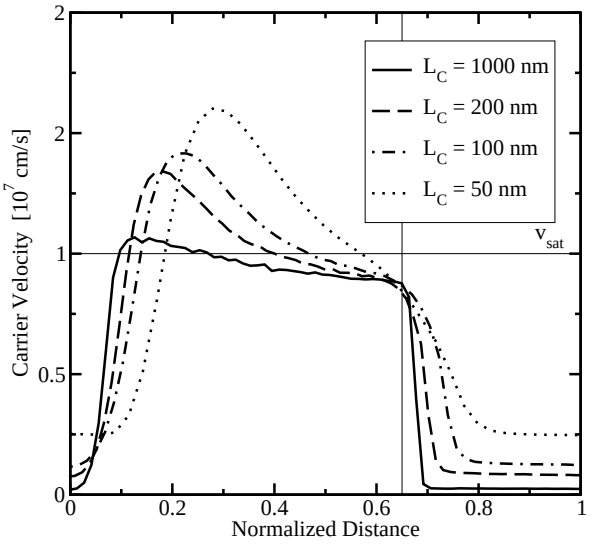

Fig. 2: A comparison of the average carrier velocities of comparable n^+-n-n^+ test structures. The velocity overshoot is caused by the non-locality of the carrier temperature.

where $\tau_{\mathcal{E}}$ is the energy relaxation time. However, for rapidly increasing electric fields the carrier temperature lags behind the electric field because it takes the carriers some time to pick up energy from the field. A consequence of the lag is that the local carrier temperature can be considerably smaller than the one predicted by the homogeneous energy flux equation. This non-locality of the carrier temperature is shown in Fig. 1 for n^+-n-n^+ test structures with varying channel lengths. To facilitate comparison the spatial coordinate has been normalized to make the electric fields of all devices overlap. The bias has been chosen to give a maximum electric field of 300 kV/cm in all devices.

An important consequence of this non-local behavior of the carrier temperature is that the lag gives rise to an overshoot in the carrier velocity as shown in Fig. 2. Also shown is the saturation velocity v_{sat} which is the maximum velocity observed in stationary bulk simulations. The reason for the velocity overshoot is that the mobility depends to first order on the energy and not on the electric field. As the mobility μ has not yet been reduced by the increased energy but the electric field is already large, an overshoot in the velocity $\mathbf{v} = \mu\mathbf{E}$ is observed until the carrier energy comes into equilibrium with the electric field again. Thus, drift-diffusion simulations predict the same velocity profile as for slowly varying fields which can dramatically underestimate the carrier velocities.

Similar to the mobility, many other physical processes like impact ionization are more accurately described by a model based on moments of the distribution function rather than a local electric field model. This is because the scattering operator in Boltzmann's transport equation depends on the distribution function and not on the electric field.

Altogether it can be noted that modeling of deep-submicron devices is becoming more and more problematic. Although successful reproduction of terminal characteristics of nano-scale MOS transistors has been reported with the drift-diffusion model [10], the values of the physical parameters used significantly violate basic physical principles. In particular, the saturation velocity v_{sat} had to be set to more than twice the value observed in bulk measurements. These solutions may provide short-term fixes to available models but obtaining 'correct' results from the wrong physics is definitely unsatisfactory in the long run.

III. ENERGY-TRANSPORT MODELS

In commercial device simulators several variants of energy-transport models are available. These models are either based on Stratton's [2] or Bløtekjær's [3] approach. Energy-transport models can be derived from Bløtekjær's hydrodynamic model by applying the diffusion approximation [11] which results in a neglect of the convective terms and the time derivatives in the flux relations. These models consider the

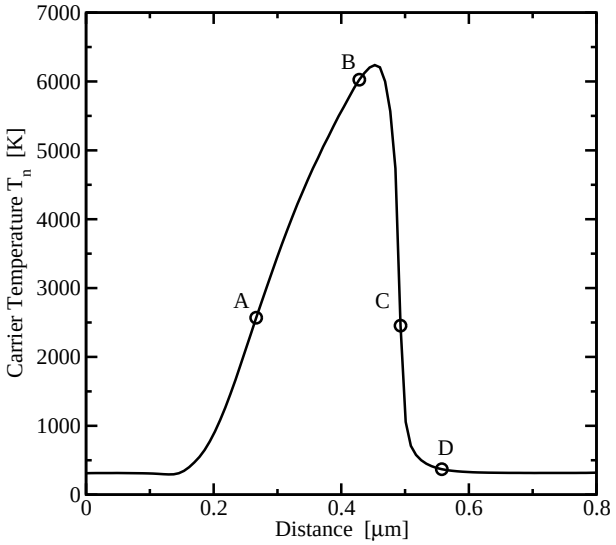

Fig. 3: Electron temperature inside an n^+-n-n^+ test structure with $L_\mathrm{c} = 200\,\mathrm{nm}$.

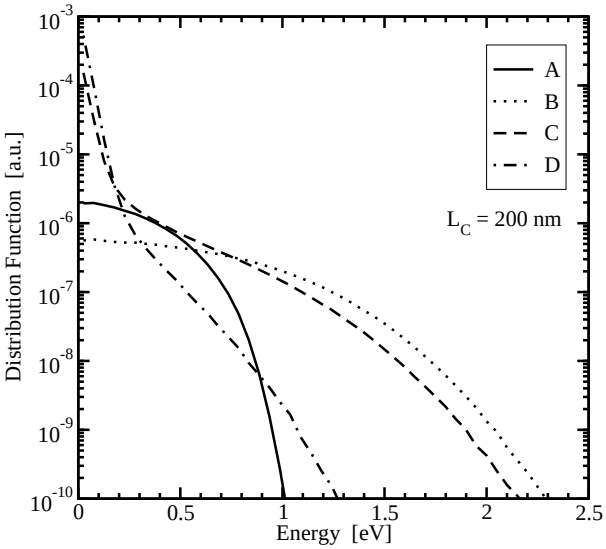

Fig. 4: The distribution function at the four characteristic points. The average energies at the points A and C are the same whereas the distribution function looks completely different. At point D, where the carrier temperature is 370 K, a significant high-energy tail exists.

first three or four moments of Boltzmann's equation and have typically the following form

$$\begin{aligned}
\nabla\cdot\mathbf{J} &= \mathrm{q}R\\
\mathbf{J} &= \mathrm{q}n\mu\mathbf{E} + \mu\mathrm{k_B}\nabla(nT_n)\\
\nabla\cdot\mathbf{S} &= \mathbf{E}\cdot\mathbf{J} - n\tfrac{3}{2}\mathrm{k_B}\frac{T_n - T_\mathrm{L}}{\tau_\mathcal{E}} + G_{\mathcal{E}_n}\\
\mathbf{S} &= -\tfrac{5}{2}\frac{\mu_S}{\mu}\frac{\mathrm{k_B}T_n}{\mathrm{q}}\mathbf{J} - \tfrac{5}{2}\frac{\mu_S}{\mu}\Big(\frac{\mathrm{k_B}}{\mathrm{q}}\Big)^2\mathrm{q}\mu n T_n\nabla T_n
\end{aligned}$$

The physical parameters are the mobility μ, the energy flux mobility μ_S and the energy-relaxation time $\tau_\mathcal{E}$. Normally, the ratio of the mobilities μ_S/μ is modeled as a constant with values in the range $[0.8, 1]$. R and $G_{\mathcal{E}_n}$ are the contributions due to generation and recombination processes.

One of the fundamental problems of energy-transport models is that only the average energy is available to model the shape of the distribution function. Therefore, a heated Maxwellian distribution is frequently assumed for the closure of the equation system and for the modeling of physical processes. This assumption is significantly violated in modern semiconductor devices. Monte Carlo simulation results of an n^+-n-n^+ test structure with a channel length of $L_\mathrm{c} = 200\,\mathrm{nm}$ are shown in Fig. 3 and Fig. 4. Even though the average energy is the same at points A and C, the distribution function looks completely different in both cases [12], [13]. A heated Maxwellian distribution, which gives a straight line in a semi-logarithmic plot, is definitely a poor approximation throughout the whole device.

IV. SIX MOMENTS MODEL

By considering the first six moments of Boltzmann's transport equation a macroscopic transport model can be derived without making any assumption on the shape of the distribution function [7] except that the diffusion approximation holds. The static flux and balance equations of the six moments model for electrons read:

$$\begin{aligned}
\nabla\cdot\mathbf{J} &= \mathrm{q}R\\
\mathbf{J} &= \mathrm{q}n\mu\mathbf{E} + \mu\mathrm{k_B}\nabla(nT_n)\\
\nabla\cdot\mathbf{S} &= \mathbf{E}\cdot\mathbf{J} - n\tfrac{3}{2}\mathrm{k_B}\frac{T_n - T_\mathrm{L}}{\tau_\mathcal{E}} + G_{\mathcal{E}_n}\\
\mathbf{S} &= -\tfrac{5}{2}\frac{\mathrm{k_B^2}}{\mathrm{q}}\frac{\mu_S}{\mu}\mu\Big(\frac{\mathrm{q}}{\mathrm{k_B}}\mathbf{E}\,n\,T_n + \nabla(n\,T_n^2\,\beta_n)\Big)\\
\nabla\cdot\mathbf{K} &= 2\,\mathrm{q}\,\mathbf{E}\cdot\mathbf{S} - \tfrac{15}{4}\,\mathrm{k_B^2}\,n\,\frac{T_n^2\,\beta_n - T_\mathrm{L}^2}{\tau_\beta} + G_{\beta_n}\\
\mathbf{K} &= -\tfrac{35}{4}\frac{\mathrm{k_B^3}}{\mathrm{q}}\frac{\mu_K}{\mu}\mu\Big(\frac{\mathrm{q}}{\mathrm{k_B}}\mathbf{E}\,n\,T_n^2\,\beta_n + \nabla(n\,T_n^3\,\beta_n^3)\Big)
\end{aligned}$$

The additional parameters are the kurtosis relaxation time τ_β and the kurtosis flux mobility μ_K. The

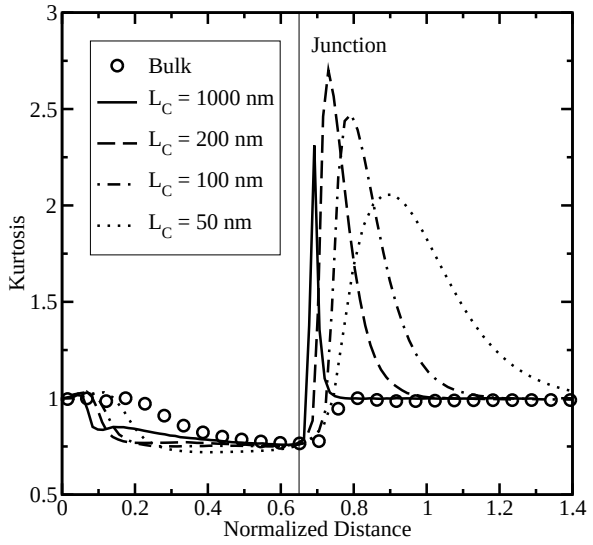

Fig. 5: The kurtosis of different n^+-n-n^+ test structures. Note the strong deviation from unity after the second junction.

unknowns of the six moments model are defined as

$$n = \langle 1 \rangle, \qquad \mathbf{J}_n = -\mathrm{q}\langle \mathbf{u} \rangle \tag{2}$$

$$T_n = \frac{2}{3\,\mathrm{k_B}} \frac{\langle \mathcal{E} \rangle}{n}, \qquad \mathbf{S}_n = \langle \mathbf{u}\, \mathcal{E} \rangle \tag{3}$$

$$\beta_n = \frac{3}{5} \frac{\langle \mathcal{E}^2 \rangle}{\langle \mathcal{E} \rangle^2}, \qquad \mathbf{K}_n = \langle \mathbf{u}\, \mathcal{E}^2 \rangle \tag{4}$$

These are the carrier concentration n, the carrier temperature T_n, the kurtosis of the distribution function β_n, the current density $\mathbf{J}_n$, the energy flux density $\mathbf{S}_n$, and the kurtosis flux density $\mathbf{K}_n$. The statistical average is defined as

$$\langle \Phi \rangle = \frac{1}{4\pi^3} \int \Phi f \; \mathrm{d}^3\mathbf{k} \tag{5}$$

where f is the distribution function and Φ the weight function.

The first four equations are the same as for the energy-transport model, except that the kurtosis β_n appears in the energy flux equation. As a consequence, the energy flux equation cannot be written in the form frequently used for energy-transport models as proportional to the current density without producing additional terms. This modification makes the coupled equation system difficult to solve and approximations have been used [6], [7]. Note, that the six moments model reduces to a standard energy-transport model when the equations for $\mathbf{K}$ are dropped and a value of unity is assumed for β_n.

A. Properties of the Kurtosis

For a heated Maxwell distribution and parabolic bands $\beta_n = \beta_\mathrm{M} = 1$. Thus a $\beta_n \neq 1$ quantifies the deviation from the Maxwellian shape in the parabolic case. When nonparabolicity is taken into account, the value of β_M depends on the energy but stays close to unity. Note, however, that a Maxwellian shape is never observed in Monte Carlo simulations, except for the contact regions where the carriers are still cold.

Typical values of the kurtosis β_n are in the range [0.75, 3] which indicates a strong deviation from a heated Maxwellian distribution. In addition, as shown in Fig. 5, the kurtosis behaves fundamentally differently than in bulk [14] where a unique relationship $\beta_\mathrm{Bulk}(T_n)$ exists. Especially at the drain side of the structures we observe a strong deviation from the Maxwellian shape. This deviation corresponds to the high-energy tail in Fig. 4.

V. APPLICATIONS

Despite the modified description of carrier transport the six moments model provides the kurtosis of the distribution function. This parameter is essential and can be used to formulate an accurate analytical model of the distribution function [15], [14]. In particular, the following model for the symmetric part of the distribution function has been proposed in [14]

$$f(\mathcal{E}) = A\Big\{\underbrace{\exp\Big[-\Big(\frac{\mathcal{E}}{\mathrm{k_B}T_\mathrm{ref}}\Big)^b\Big]}_{f_1(\mathcal{E})} + c\underbrace{\exp\Big[-\frac{\mathcal{E}}{\mathrm{k_B}T_2}\Big]}_{f_2(\mathcal{E})}\Big\} \tag{6}$$

The parameters T_ref, b, and c are determined in such a way that (6) selfconsistently reproduces T_n and β_n. With reasonable accuracy the temperature of the cold Maxwellian distribution T_2 can be assumed to equal the lattice temperature [14]. Many models given in literature violate the important issue of selfconsistency [16] which introduces unpredictable errors.

A comparison of (6) with Monte Carlo data is given in Fig. 6 for two critical regions of an n^+-n-n^+ test structure with $L_\mathrm{c} = 200\,\mathrm{nm}$. In the channel region, the high-energy tail is much less populated than would be predicted by a heated Maxwellian distribution. This is accounted for by f_1 and c is assumed to be zero. In the drain region, the cold carriers from the drain appear clearly in the distribution function which is modeled via f_2. Note that models based solely on the average energy cannot predict this tail because the average energy is dominated by the cold carriers. Information about the high energy tail is available in the kurtosis (cf. Fig. 5).

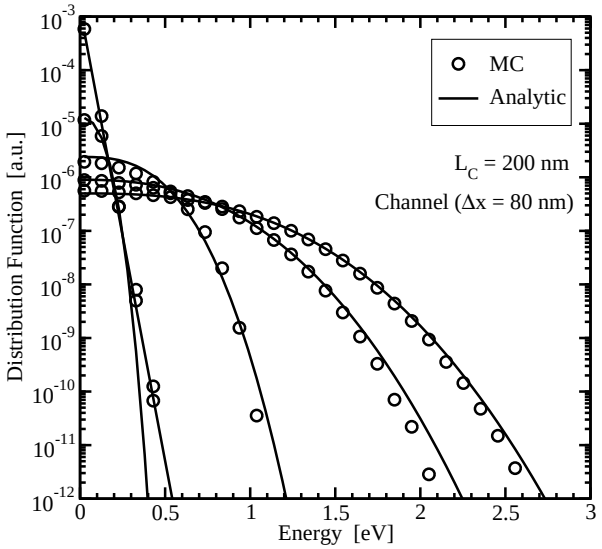

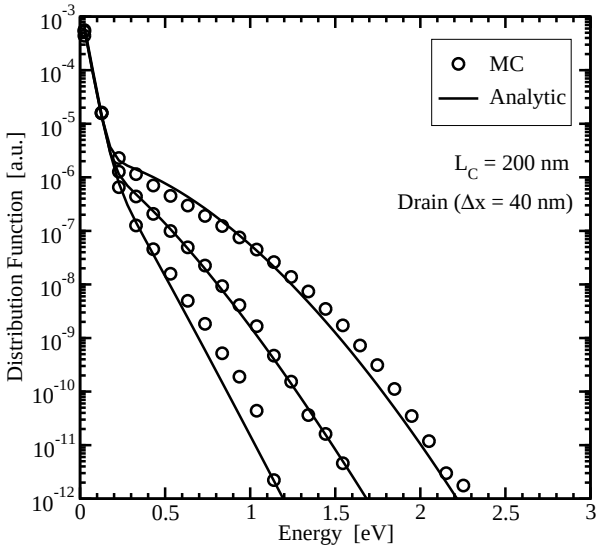

Fig. 6: The analytic distribution function inside the 'channel' and the 'drain-region' of an n^+-n-n^+ test structure with $L_c = 200\,\mathrm{nm}$. The spacing between the DFs is given as Δx.

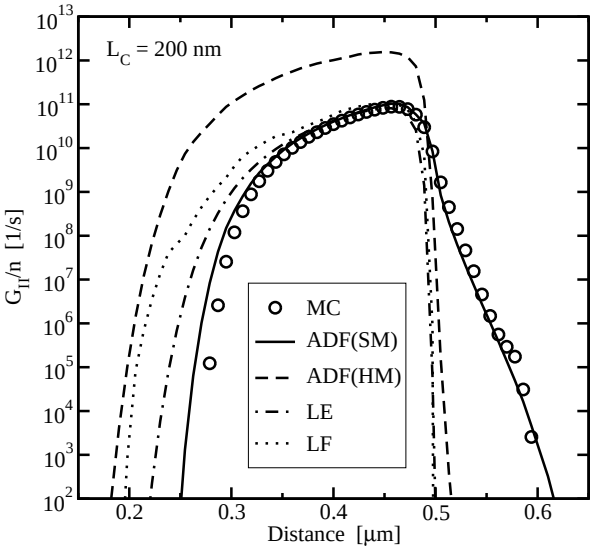

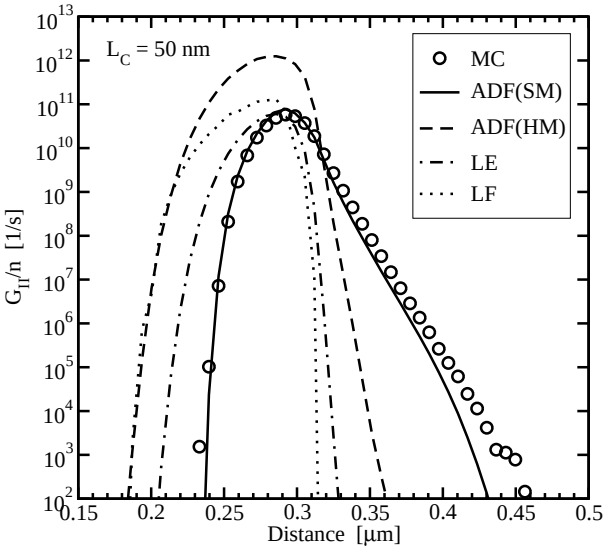

Fig. 7: Analytical impact ionization rates in comparison with Monte Carlo data for two n^+-n-n^+ test structures. The ADF models use analytical models for the distribution function, either based on six moments (SM) or a heated Maxwellian distribution (HM). Also shown are the empirical models based on the local field (LF) and the local energy (LE).

A. Impact Ionization

For reliability issues and for the calculation of substrate currents an accurate model for impact ionization is required. The analytic distribution function (6) can be used to transfer microscopic impact ionization rates into macroscopic models. A comparison with Monte Carlo data is shown in Fig. 7 where the analytical models have been evaluated using values from the Monte Carlo simulation. The model based on (6) delivers highly accurate results for both devices. It is important to note, that when a heated Maxwellian is assumed instead of (6), the results deteriorate. This is frequently done in physics based models [17]. Also shown are the results obtained by two commonly used empirical fit models [18]

$$G_{\mathrm{II}}^{\mathrm{LF}} = n\, g_{\mathrm{II}}\, \exp\Big(-\frac{E_C}{|\mathbf{E}|}\Big) \tag{7}$$

$$G_{\mathrm{II}}^{\mathrm{LE}} = n\, g_{\mathrm{II}}\, \exp\Big(-\frac{\mathcal{E}_C}{\mathrm{k_B}\, T_n}\Big) \tag{8}$$

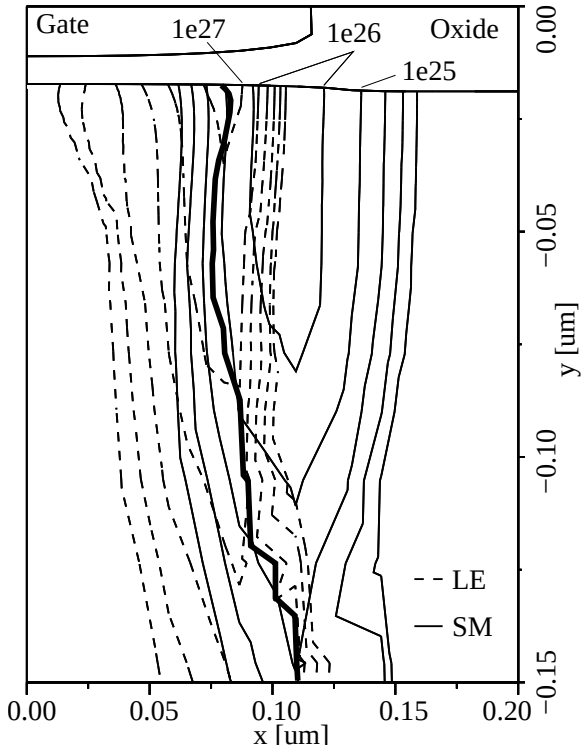

Fig. 8: Comparison of the impact ionization rate as predicted by a local energy model (LE) and by a six moments model (SM). Also shown is the metallurgic junction (fat line).

These models are based on the local field (LF) and on the local energy (LE). To match the Monte Carlo results the LF and LE models have been calibrated, whereas the same parameters as in the Monte Carlo simulation where used for the models based on the analytical distribution function.

For the purpose of demonstration we considered two MOSFETs with gate-lengths $L_{\mathrm{g}} = 1.0\,\mu$m and $L_{\mathrm{g}} = 0.25\,\mu$m [19]. A comparison of the impact ionization rate predicted by a local energy model and by a six moments model is given in Fig. 8 for the short-channel device. Also shown is the metallurgic junction (fat line). For the local energy model the maximum impact ionization rate occurs at the junction where the average energy rapidly decreases because the hot carriers from the channel meet the large pool of cold carriers in the drain. In the case of the six moments model, the maximum is inside the drain region which is in agreement with Monte Carlo simulations.

Simulated substrate currents for both devices are given in Fig. 9. Both characteristics were calculated using the same parameter values. The local energy model had to be calibrated for these devices.

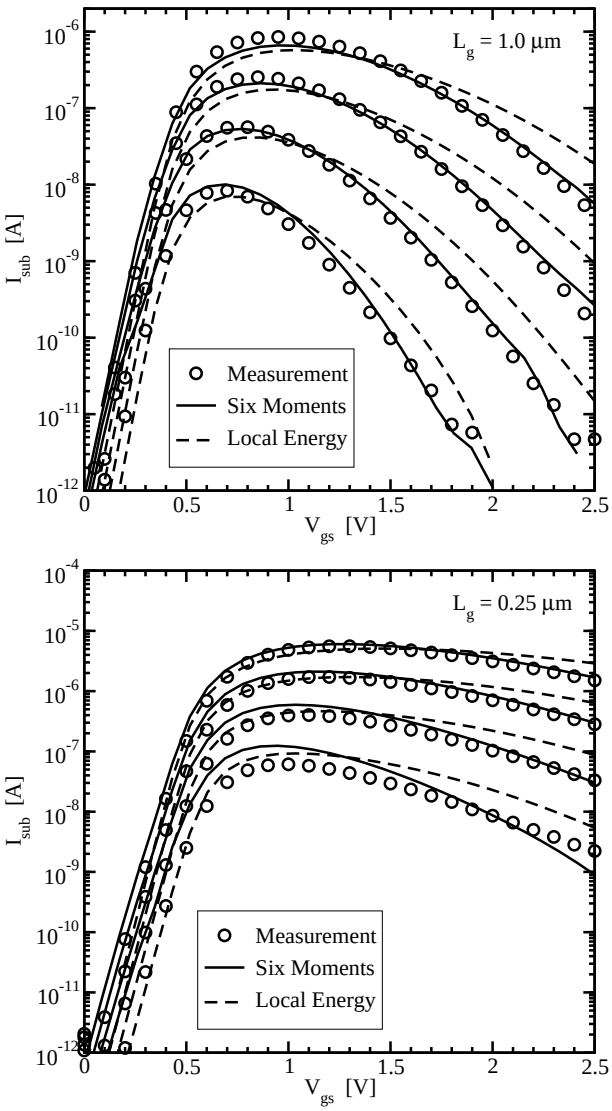

Fig. 9: Comparison of simulated substrate currents and measurements for the two MOS transistors.

Although reasonable substrate currents are delivered by the local energy model, the calculated ionization profiles *inside* the devices are at the wrong position and have a wrong shape which requires individual calibration.

B. Hot-Carrier Gate Currents

For the design of sub-micron devices with gate oxide thicknesses around or below 2 nm, accurate prediction of gate oxide tunneling currents is of increasing importance. Thermionic emission based models are frequently used for this purpose [16]. These models require detailed knowledge of the distribution function. Frequently, a heated Maxwellian distribution is assumed which leads to erroneous results. In

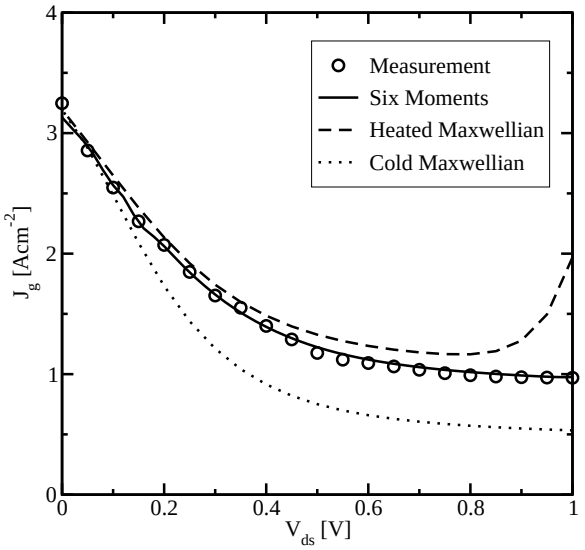

Fig. 10: Gate current density as a function of the drain bias for three different analytic distribution functions. Also shown is the measured data.

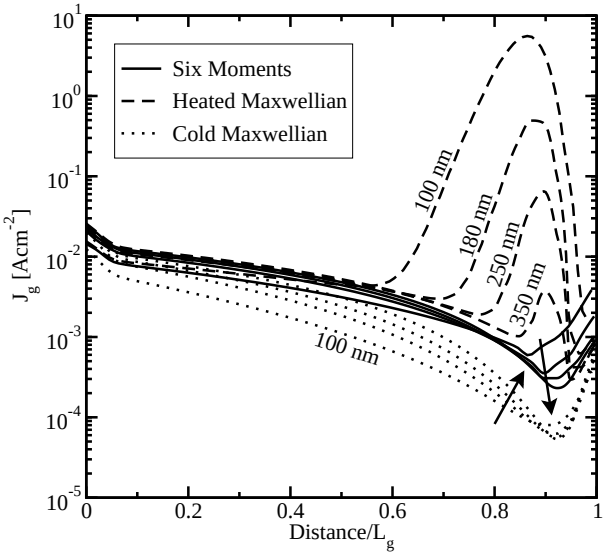

Fig. 11: Spatial distribution of the gate current density for different gate lengths with an oxide thickness of 2.6 nm. The arrows indicate an increase of the gate length in the same manner as for the heated Maxwellian distribution.

particular, such models lead to a massive overestimation of gate currents especially for devices with small gate lengths.

Following [16], the gate current density is given as

$$J_{\mathrm{g}} = \int_0^\infty f(\mathcal{E})\, g(\mathcal{E})\, v_\perp(\mathcal{E})\, T(\mathcal{E})\, \mathrm{d}\mathcal{E} \qquad (9)$$

where $f(\mathcal{E})$ is the electron energy distribution function, $g(\mathcal{E})$ the density of states, $v_\perp(\mathcal{E})$ the electron velocity perpendicular to the interface, and $T(\mathcal{E})$ the tunneling probability. A simple model for the tunneling probability $T(\mathcal{E})$ can be derived using the WKB approximation [20] for trapezoidal and triangular barriers:

$$T(\mathcal{E}) = \exp\left\{-4\frac{\sqrt{2m_{ox}}}{3\hbar q F_{ox}} \cdot \phi\right\} \qquad (10)$$

The barrier ϕ is given as

$$\phi = \begin{cases} (\Phi - \mathcal{E})^{3/2} & \Phi_0 < \mathcal{E} < \Phi \\ (\Phi - \mathcal{E})^{3/2} - (\Phi_0 - \mathcal{E})^{3/2} & \mathcal{E} < \Phi_0 \end{cases}$$

where Φ and Φ_0 are the upper and lower barrier height, and F_{ox} is the electrostatic field in the oxide layer. As a first order correction to the single parabolic band model, we use Kane's dispersion relation [21] for the density of states $g(\mathcal{E})$. For the distribution function, (6) is used. The velocity perpendicular to the interface can be derived from [22] as $v_\perp(\mathcal{E}) = (\partial\mathcal{E}/\partial p)/4$.

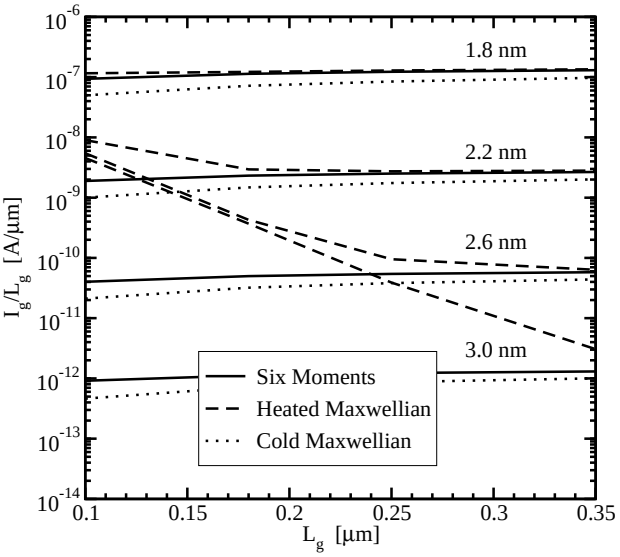

Fig. 12: Gate current normalized to the gate length for different gate oxide thicknesses.

For the evaluation of the tunnel currents (9) we solve the six moments model for several MOS transistors with varying gate lengths and oxide thicknesses. In Fig. 10 the effect of the drain voltage on the gate current is shown for a MOS transistor with $L_{\mathrm{g}} = 0.4\,\mu$m and an oxide thickness of 1.8 nm. The measured data was taken from [23] and compared to the analytic expression (9). To estimate the influence

of the distribution function, (9) was evaluated using three different analytic models. When a heated Maxwellian distribution is assumed a spurious gate current is obtained for higher drain voltages. Interestingly, a cold Maxwellian distribution gives much better results but systematically underestimates the gate current. The analytic distribution function (6) exactly reproduces the measurements.

The error obtained from the heated Maxwellian distribution is due to the overestimation of the high-energy tail of the distribution function. Even though the effect is relatively small in Fig. 10, it becomes more pronounced when the gate length is reduced. This is shown in Fig. 11 where the error reaches four orders of magnitude for a gate length of 100 nm. The bias voltages were not scaled and all devices where biased with $V_{\mathrm{gs}} = 1\,\mathrm{V}$ and $V_{\mathrm{ds}} = 1\,\mathrm{V}$. Therefore, the maximum temperatures occurring inside the devices increase when the gate length is reduced. An estimation shows that these spurious gate currents occur when the temperature in the channel reaches approximately 1000 K, a value easily exceeded in state-of-the-art devices.

In Fig. 12 the influence of the distribution function model on the gate current is shown where the gate length and the oxide thickness have been varied. For the Maxwellian approximation $I_{\mathrm{g}}/L_{\mathrm{g}}$ becomes even independent of the oxide thickness which seems questionable.

VI. CONCLUSION

Various transport models have been considered so far. Apart from the drift-diffusion model higher-order models based on either Stratton's or Bløtekjær's approach have been considered. However, the examples presented here indicate that the average energy is not sufficient for an accurate description of hot-carrier phenomena. We present a particular solution using a six moments transport models which also includes the kurtosis of the distribution function. The kurtosis allows for a significant improvement in the accuracy of hot-carrier models.

References

[1] D. Scharfetter and H. Gummel, "Large-Signal Analysis of a Silicon Read Diode Oscillator," *IEEE Trans.Electron Devices*, vol. 16, no. 1, pp. 64–77, 1969.

[2] R. Stratton, "Diffusion of Hot and Cold Electrons in Semiconductor Barriers," *Physical Review*, vol. 126, no. 6, pp. 2002–2014, 1962.

[3] K. Bløtekjær, "Transport Equations for Electrons in Two-Valley Semiconductors," *IEEE Trans.Electron Devices*, vol. 17, no. 1, pp. 38–47, 1970.

[4] R. Thoma, A. Emunds, B. Meinerzhagen, H. Peifer, and W. Engl, "Hydrodynamic Equations for Semiconductors with Nonparabolic Band Structure," *IEEE Trans.Electron Devices*, vol. 38, no. 6, pp. 1343–1353, 1991.

[5] T.-W. Tang, S. Ramaswamy, and J. Nam, "An Improved Hydrodynamic Transport Model for Silicon," *IEEE Trans.Electron Devices*, vol. 40, no. 8, pp. 1469–1476, 1993.

[6] K. Sonoda, M. Yamaji, K. Taniguchi, C. Hamaguchi, and S. Dunham, "Moment Expansion Approach to Calculate Impact Ionization Rate in Submicron Silicon Devices," *J.Appl.Phys.*, vol. 80, no. 9, pp. 5444–5448, 1996.

[7] T. Grasser, H. Kosina, M. Gritsch, and S. Selberherr, "Using Six Moments of Boltzmann's Transport Equation for Device Simulation," *J.Appl.Phys.*, vol. 90, no. 5, pp. 2389–2396, 2001.

[8] S. Selberherr, *Analysis and Simulation of Semiconductor Devices*. Wien–New York: Springer, 1984.

[9] G. Wachutka, "Rigorous Thermodynamic Treatment of Heat Generation and Conduction in Semiconductor Device Modeling," *IEEE Trans.Computer-Aided Design*, vol. 9, no. 11, pp. 1141–1149, 1990.

[10] J. Bude, "MOSFET Modeling into the Ballistic Regime," in *Proc. Simulation of Semiconductor Processes and Devices*, (Seattle, Washington, USA), pp. 23–26, Sept. 2000.

[11] C. Ringhofer, C. Schmeiser, and A. Zwirchmayer, "Moment Methods for the Semiconductor Boltzmann Equation in Bounded Position Domains," *SIAM J.Numer.Anal.*, vol. 39, no. 3, pp. 1078–1095, 2001.

[12] S.-C. Lee and T.-W. Tang, "Transport Coefficients for a Silicon Hydrodynamic Model Extracted from Inhomogeneous Monte-Carlo Calculations," *Solid-State Electron.*, vol. 35, no. 4, pp. 561–569, 1992.

[13] G. Wolokin and J. Frey, "Overshoot Effects in the Relaxation Time Approximation," in *Proc.NASECODE VIII*, (Vienna), pp. 107–108, 1992.

[14] T. Grasser, H. Kosina, C. Heitzinger, and S. Selberherr, "Characterization of the Hot Electron Distribution Function Using Six Moments," 2001. submitted to *J.Appl.Phys.*

[15] K. Sonoda, S. Dunham, M. Yamaji, K. Taniguchi, and C. Hamaguchi, "Impact Ionization Model Using Average Energy and Average Square Energy of Distribution Function," *Jap.J.Appl.Phys.*, vol. 35, no. 2B, pp. 818–825, 1996.

[16] K. Hasnat, C.-F. Yeap, S. Jallepalli, S. Hareland, W.-K. Shih, V. Agostinelli, A. Tasch, and C. Maziar, "Thermionic Emission Model of Electron Gate Current in Submicron NMOSFETs," *IEEE Trans.Electron Devices*, vol. 44, no. 1, pp. 129–138, 1997.

[17] W. Quade, E. Schöll, and M. Rudan, "Impact Ionization within the Hydrodynamic Approach to Semiconductor Transport," *Solid-State Electron.*, vol. 36, no. 10, pp. 1493–1505, 1993.

[18] K. Souissi, F. Odeh, H. Tang, A. Gnudi, and P. Lu, "Investigation of the Impact Ionization in the Hydrodynamic Model," *IEEE Trans.Electron Devices*, vol. 40, no. 8, pp. 1501–1507, 1993.

[19] T. Grasser, H. Kosina, M. Gritsch, and S. Selberherr, "Accurate Simulation of Substrate Currents by Accounting for the Hot Electron Tail Population," in *Proc. of the 30th European Solid-State Device Research Conference*, (Nuremberg, Germany), pp. 215–218, Sept. 2001.

[20] R. Shankar, *Principles of Quantum Mechanics*. Plenum Press, New York, 1994.

[21] E. Kane, "Band Structure of Indium Antimonide," *J.Phys.Chem.Solids*, vol. 1, pp. 249–261, 1957.

[22] C. Fiegna, F. Venturi, M. Melanotte, E. Sangiorgi, and B. Riccó, "Simple and Efficient Modeling of EPROM Writing," *IEEE Trans.Electron Devices*, vol. 38, no. 3, pp. 603–610, 1991.

[23] S. Schwantes and W. Krautschneider, "Relevance of Gate Current for the Functionality of Deep Submicron CMOS Circuits," in *Proc. of the 30th European Solid-State Device Research Conference*, (Nuremberg, Germany), pp. 471–474, Sept. 2001.